Preprint
UCRL-JC-138111

X-ray Sources Generated from Gas-Filled Laser-Heated Targets

C.A. Back, J. Grun, C.D. Decker, J. Davis, J.M. Laming, U. Feldman, L.J. Suter, O.L. Landen, M. Miller, F. Serduke, and C. Wuest

This article was submitted to
12th American Physical Society Topical Conference on Atomic Processes in Plasmas, Reno, NV, March 19 – 24, 2000

June 6, 2000

X-ray Sources Generated from Gas-filled Laser-Heated Targets

C. A. Back, J. Grun[a], C. D. Decker, J. Davis[b], J. M. Laming[a], U. Feldman[a], L. J. Suter, O. L. Landen, M. Miller, F. Serduke, C. Wuest

Lawrence Livermore National Laboratory, L-21, P.O. Box 808, Livermore, CA 94551

[a] *Naval Research Laboratory, 4555 Overlook Ave, S.W., Washington, D. C. 20375*

[b] *Alme & Associates, 6020 Richmond Hwy., Ste 204, Alexandria, VA*

Abstract. The X-ray sources in the 4-7 keV energy regime can be produced by laser-irradiating high-Z gas-filled targets with high-powered lasers. A series of experiments have been performed using underdense targets that are supersonically heated with ~ 35 kJ of 0.35 μm laser light. These targets were cylindrical Be enclosures that were filled with 1-2 atms of Xe gas. L-shell x-ray emission is emitted from the plasma and detected by Bragg crystal spectrometers and x-ray diodes. Absolute flux measurements show conversion efficiencies of ~ 10% in the multi-kilovolt x-ray emission. These sources can be used as bright x-ray backlighters or for material testing.

INTRODUCTION

Multi-keV x-ray sources can be routinely produced at high-powered laser facilities. In the last ten years, they have been extremely useful in the radiography of high energy density laser-produced plasmas. Now, we are focussing on research to develop the sources themselves for more tailored applications. In particular, new applications for material testing are motivating the development of sources at even higher photon energies. Furthermore, as hotter and denser states of matter are created, high flux radiography sources will need to be at harder x-ray energies. Recent experiments in which a confined gas is supersonically heated by a laser have shown that up to 10% of the energy can be converted into multi-keV x-rays. In this paper we discuss research behind developing more efficient radiators.

The essential characteristics of x-ray sources include:

1. brightness
2. frequency distribution
3. temporal duration
4. size of the source
5. spatial uniformity

In general maximum brightness is always desirable. However, the frequency distribution and temporal duration of any particular source are determined by the application of interest. For ICF, sources have a near-blackbody frequency distribution, on the order of ns, and can either be constant in intensity, or shaped to optimize implosion trajectories. For radiography, maximum brightness in a limited bandwidth is needed with both long and short duration backlighting applications. In addition, a small source size may be important to minimize spatial blurring of the image in point projection applications. Or, a large uniform source size may be desirable for area backlighters [1, 2].

Material testing and radiography require high flux at hard x-ray energies. The conversion of laser energy into useable x-rays is quantified in conversion efficiency measurements where the total energy that is emitted by the source in a particular spectral bandwidth is divided by the absorbed laser energy. Many conversion efficiency studies have focussed on sub-keV x-ray range [3-5]. Those studies have been motivated by indirect inertial confinement fusion (ICF) where near local thermodynamic equilibrium (near-LTE) radiation sources drive implosions. For ICF applications, the radiation drive is produced inside of hohlraums, cylindrical or spherical cavities that are irradiated by a laser. The frequency distribution of the source is nearly Planckian, peaking at ~ 2.8 kT_e and the energy is often characterized by σT^4 where σ is the Stefan-Boltzmann coefficient and T is an effective blackbody radiation temperature. At multi-keV energies, even high-powered lasers creating blackbody sources with frequency distributions that peak at multi-keV photon energies is difficult. Therefore, x-ray source development for material testing and radiography must concentrate on non-LTE sources.

Backlight and radiative sources are typically produced by irradiating disk targets, or hohlraum targets. For solid disks, the conversion efficiency has been studied as a function of laser intensity, laser wavelength, laser pulse length, and target material. These studies have produced an experimental database of conversion efficiencies [6-9]. Data from many different laboratories show a steep decline in conversion efficiency with photon energy. Overall, the fraction emitted in multi-keV x-rays is < 1%, even though the total conversion efficiency integrated over all photon energies may be significant, especially for higher Z elements [10].

Apart from experimental studies to measure conversion efficiency, research to optimize the sources has been limited. The most significant increase in conversion efficiency to date was achieved by increased coupling of the laser energy into the target by using a shorter laser wavelength. Some source characteristics can be controlled. For example techniques to limit the spot size include the use of microdots or multilayer targets in which an overcoat tamps the radial expansion of the plasma [11, 12]. However, the typical physical characteristics of multi-keV sources generated from disk targets are limited in size to the area of the target illuminated and duration to the temporal duration of the laser pulse.

We have developed an alternative target which relies on laser-heating gas-filled targets [13, 14]. These targets are supersonically heated by inverse bremsstrahlung, which produces an underdense plasma. By underdense we mean that electron density in the plasma, n_e, is less than the critical density of the laser in cm^{-3}, $n_c = 1.1 \times 10^{21} \lambda^2$, where λ is the wavelength of the laser in microns. Laser energy is then absorbed through collisional damping of the laser light wave.

The high conversion efficiency of these targets is due to optimization of the initial target conditions and laser parameters to produce high temperature plasmas. Laser energy coupling into the target is still important. However, as long as initial conditions are controlled to ensure supersonic heating with minimum backscatter, future advanced designs for gas-filled targets can be more focussed on design of the target, i.e. the choice of gas, and use of hydrodynamic motion to maximize the emission. Laser-produced plasma sources have advantages over other x-ray sources because the target design and laser irradiation conditions can be optimized to create the source.

MULTI-KILOVOLT CONVERSION EFFICIENCY

The basic advantages of a gas target over a disk target in generating multi-keV x-rays can be shown by one-dimensional calculations. For comparison, the underdense radiator is represented by a cylindrical gas column. In figure 1, the temperature and density gradients for an underdense radiator at 0.01 g/cc are compared to a dense solid disk-like target at 0.1 g/cc. In both figures, the laser is incident from the right to a target at z=0. Multi-keV emission is typically created in high temperature regions where the heated material becomes highly ionized. For disk-like targets, the density steeply falls as the plasma expands from the surface of the target in the positive z direction. For an underdense radiator where the laser has propagated in ~ 1 mm the electron density of plasma for $n_e > 10^{21}$ cm^{-3} and temperatures > 5 keV has significantly increased.

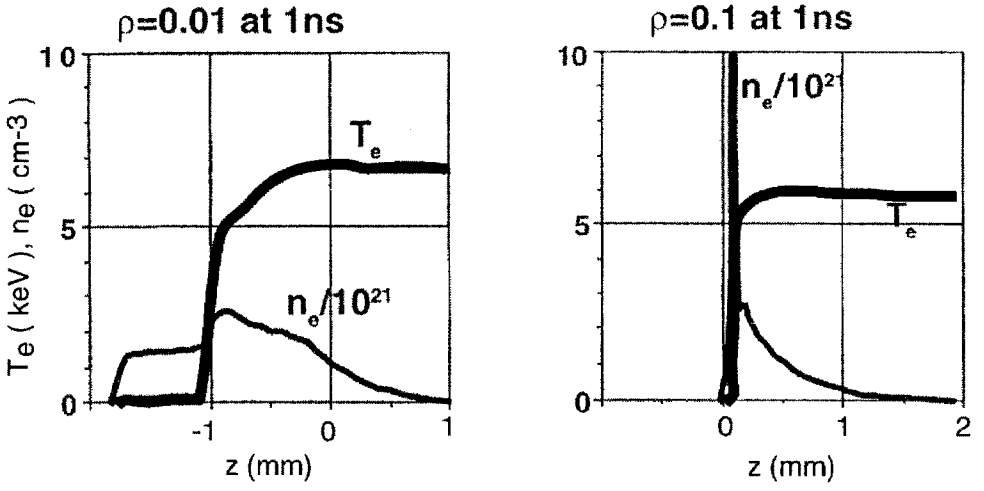

FIGURE 1. Examples of plasma gradients generated in gas targets (left) and solid disk targets (right). These one-dimensional calculations show an increased volume of low density plasma in the gas target which attains temperatures sufficient for producing multi-keV x-rays.

These sources are efficient because an increased volume of plasma at approximately 10^{21} cm^{-3} is created. The length over which energy is deposited is determined by the inverse bremsstrahlung length, L, where Z is the ionic charge (neutral = 0), ln Λ is the Coulomb logarithm, λ is the laser wavelength in μm, and T_e is the electron temperature in keV, n_e is the electron density in cm^{-3}, and n_c is the critical density in cm^{-3} [15].

$$L = \frac{0.56\,\lambda_L^2\,T_e^{3/2}}{\left(n_e/n_c\right)^2 Z \ln(\Lambda)}\sqrt{1-\left(n_e/n_c\right)}$$

For Xe-filled targets discussed below, plasma conditions produce an average ionic charge of 44, n_e = 0.1 n_c, and an electron T_e ~ 5 keV. For a Coulomb logarithm ln Λ = 8, the absorption length is ~ 0.5 mm.

The calculated overall energy balance reveals why these sources can achieve such high conversion efficiency. In figure 2, we plot the absorbed laser energy partitioned into electron thermal energy, kinetic energy, ion thermal energy, and reradiated energy for a gas-filled Xe target and a solid Ti disk target.

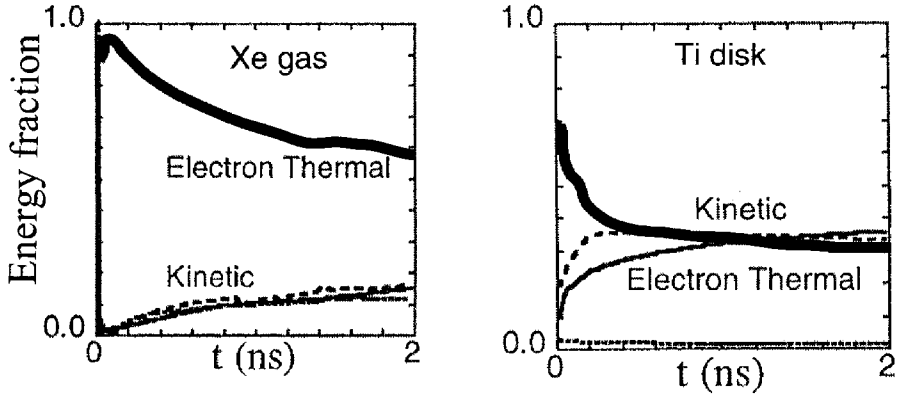

FIGURE 2. The energy balance of a gas-filled target and a traditional solid disk target. Compared to the disk target, the fraction of thermal energy (thick solid line) in the gas-filled target is increased at the expense of the kinetic energy (dotted line).

The kinetic energy is given by $1.5\ m_e v_e^2 + 1.5\ m_i v_i^2$ while the thermal energy of the plasma is $1.5\ n_e kT_e$ or , $1.5\ n_e kT_i$ for the electron or ions, respectively. From these calculations, we find that gas-filled targets are much more efficient at increasing the temperature in the plasma, thereby increasing the thermal energy in the plasma at the expense of the kinetic energy of the plasma. The higher temperature means that more energy is expended ionizing and heating the gas. This leads to an increased fraction of energy reemitted by these plasmas. Thus the heating of underdense gas-filled targets creates plasma conditions that are more optimized for multi-keV radiators.

Furthermore, the supersonic heating and underdense gas eliminate the ablative subsonic heating that occurs in solid disk targets. The thin solid line in figure 2 represents the total radiated energy. Although the total radiated energy is larger in the disk target, this is deceptive since a large fraction is sub-keV x-rays generated in the denser ablative part of the target. The reduction in soft (sub-keV) x-ray emission can be seen in figure 3 where the emission as a function of photon energy is plotted for the Xe-gas and a Ti disk.

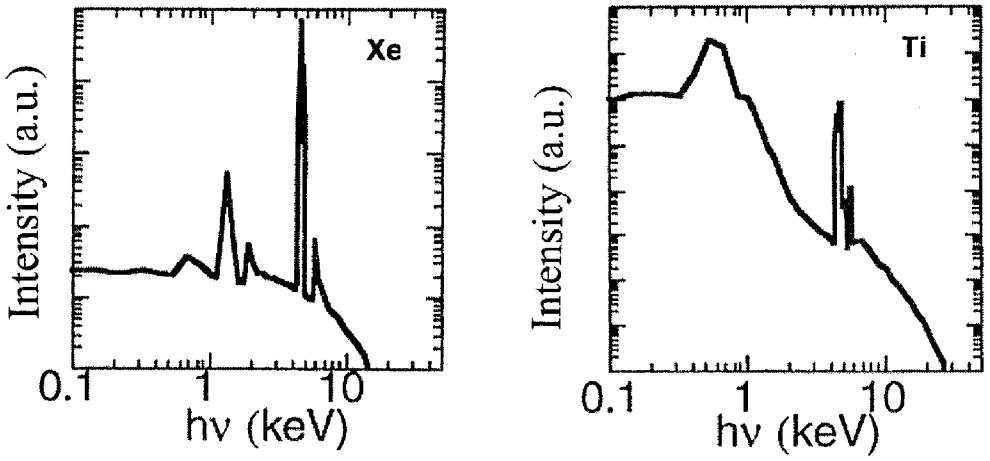

Figure 3. Calculations of the spectra emitted from the gas-filled target and disk x-ray sources. The gas-filled target has a larger fraction of multi-keV x-rays due to the strong L-shell emission of the ionized high-Z gas. The disk target emission peaks in the sub-keV region due to low temperature dense plasma in the conversion layer of the plasma.

The spectra shown in figure 3 are calculated using an average atom model. L-shell emission is complex; therefore simplified atomic models are often used in calculating the emission in hydrodynamic simulations. These codes are not spectroscopically accurate. However to first order, the energy balance in the target is insensitive to the photon energies, so the trend in the relative weightings of the sub-

keV and multi-keV energies are meaningful. Calculations of the x-ray using a more detailed atomic model can produce ~ 25 % differences in absolute flux [16]. For the Ti disk, the high density plasma in the conversion layer is primarily heated by conduction and its radiation peaks at 0.6 keV. Calculations of the gas-filled target show that the emission of the L-shell at ~ 4.8 keV dominates the sub-keV emission. Therefore, the fraction of thermal energy in the target, which is associated with the low temperature, sub-keV emission, is smaller. For plasma conditions at 5 keV in the calculations shown below, the plasma can be approximated by a coronal model because its temperature is in the range of 1 to 3 times the ionization energy of the dominant ions in emission, 4.8-5.4 keV for L-shell Xe.

EXPERIMENTAL RESULTS

Experiments were performed on the Nova laser which delivered ~ 35 kJ of 0.35 μm laser light in a 2-ns flat-topped intensity pulse. The targets were 1.6 mm long, 2.0 mm diameter Be cylinders with 100 μm thick cylindrical walls and 50 μm thick endcaps. This wall material is low Z and provides little attenuation of the emission > 2 keV. Each endcap had a laser entrance hole (LEH) that was 1.5 mm in diameter and covered with a 0.35 μm thick polyimide windows ($C_{14}H_6N_2O_4$) to confine the Xe gas. Five laser beams enter through each of the two LEH. Each beam produces a diverging focal spot of ~ 580 μm at the wall with an average intensity of $8 \times 10^{14} W/cm^2$. Figure 4 shows a cross-section of the target with the laser beams entering through the LEHs.

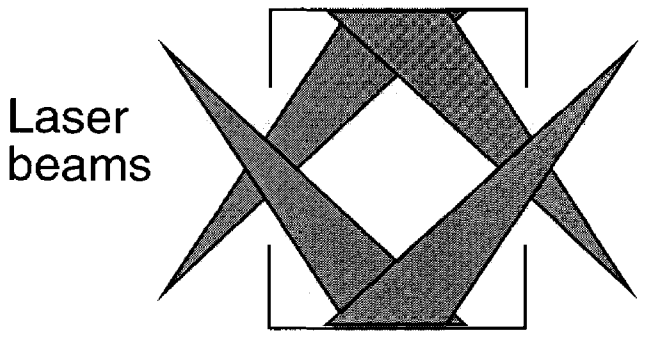

FIGURE 4. Schematic of a Xe gas-filled Be enclosure. The laser enters through holes in the endcaps. Thin polyimide membranes confine the gas inside and can withstand pressures of ~ 2 atm.

The targets had gas fills of 80% Xe and 20 % Kr. The primary gas of interest is the Xe and the Kr was mixed in to act as a tracer element to examine the feasibility of a Kr K-shell spectroscopic diagnostic. In simulations, the presence of the tracer did not affect the hydrodynamics of the target. The initial density of these plasmas is well known due to high accuracy gas pressure measurements. With a nominal 1 atm gas-fill pressure, the 5 mm^3 volume contains 2.5 $x10^{19}$ molecules. When ionized, this pressure translates to an electron density of approximately $1x10^{21}$ cm^{-3}, which is 0.1 n_c. In the series of targets discussed here pressures averaged 1.05 atm ± 5% at shot time.

A full complement of diagnostics obtained both time-integrated and time-resolved data of the emission. The primary diagnostics included time-integrated Bragg crystal spectrometer, which provides absolute measurements of the spectra, and x-ray diodes which measure the temporal history of the integrated flux. Two-dimensional x-ray images of the source were also obtained by gated x-ray diagnostics.

The Bragg crystal spectrometers record spectrally-resolved absolute flux. On each piece of data, we obtain three regions of exposure that are differentially filtered by cold x-ray filters. With different Ti, V, and Al filter attenuations, we are able to cover a dynamic range of ~ 20 to measure the weak and strong line intensities on a single shot. The spectroscopic identification of the lines shows prominent Ne-like n=3-2 and n= 4-2 emission. To obtain conversion efficiency measurements, the time-integrated spectrum is spectrally integrated over the 4-7 keV energy range to obtain the total energy emitted in the L-shell radiation from the plasma.

Data is converted from exposure to flux by taking into account the transmission of x-ray filters, the sensitivity of x-ray film, and the Bragg crystal reflectivities. The thin filters were calibrated by spot measurements using a stationary x-ray anode source as well as by checking for self-consistency in the attenuation of different exposure regions. We used the published calibrations of Henke et al. [17] for DEF x-ray film to convert from exposure to flux. The overall error bar on these measurements is ~ 25 %.

Figure 5 shows an example of the experimental spectrum measured by a Bragg crystal spectrometer. From the Bragg crystal spectra, we can also experimentally determine the T_e. A temperature diagnostic using the Na-like satellite to the Ne-like resonance line of the n = 4-2 transitions has been identified by kinetics modeling of Xe plasmas [18]. The laser heating produces an immediate onset of emission, which monotonically grows and peaks near the end of the pulse. Since, equilibration times between the excited states of the ionized Xe are on the order of tens of ps and the gas is supersonically heated, the time-integrated ratio should provide a reasonable temperature measurement. The ratio of these n = 4-2 lines give values between 0.5 and 0.8 which corresponds to an electron temperature range of 4.5 to 5.5 keV. Kr diagnostics were also consistent with this temperature range, but spectral dispersion of the ~ 13 keV K-shell lines was not sufficient for a more precise determination.

Also shown on the left-hand axis of figure 5 is the total energy integrated over the photon energy range. The total integrated energy in the 4-7 keV range divided by the laser energy absorbed is defined as the conversion efficiency.

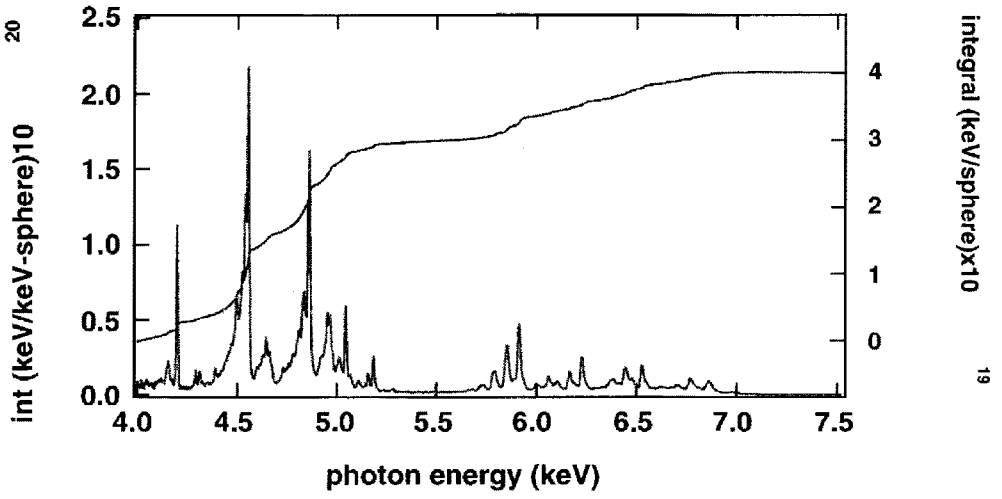

FIGURE 5. Example of the spectrum recorded from the gas-filled Xe target.

X-ray pinhole cameras provide images of the x-ray source size that are integrated over ~ 80 ps. The bleaching wave formed by the laser creates a high temperature sufficient to ionize Xe to L-shell in the plasma quickly. L-shell emission begins instantaneously and 2-D images show the entire volume emitting 0.3 ns into the 2 ns pulse for photon energies greater than 4 keV. Images at photon energies greater than 13 keV do show spatial variations related to the plasma heating. Simulations predict that in these plasmas, approximately 90 % of the laser energy is absorbed in the plasma.

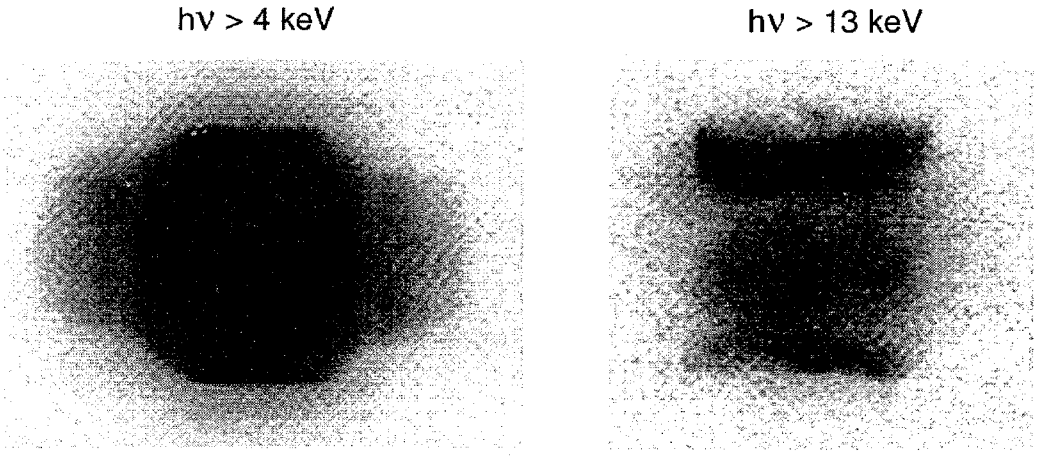

FIGURE 6. Example of x-ray images recorded simultaneously from the gas-filled target at 1.3 ns after the beginning of a 2 ns laser pulse.

Figure 7 shows a compilation of the conversion efficiencies of multi-keV x-rays measured by different laboratories. The conversion efficiency from laser-produced x-ray sources is usually measured in photon energy ranges where bound-bound emission is dominant. Due to the nuclear charge of high-Z ions the K-shell emission of a higher atomic number elements is emitted at high photon energies than the K-shell of a lower atomic number element. For instance K-shell emission of Al is ~ 1.6 keV, whereas the K-shell emission of Ti is ~ 4.7 keV. Therefore for emission from the same shell, higher photon energy data points correspond to higher atomic number targets. Significant bound-bound emission for x- ray photon energies > 4 keV is generated in K-shell emission for atomic numbers > 20 or in L-shell emission for Z > 53. Also included are the results from these Xe experiments shown as circles. These conversion efficiencies are significantly higher than the disk targets.

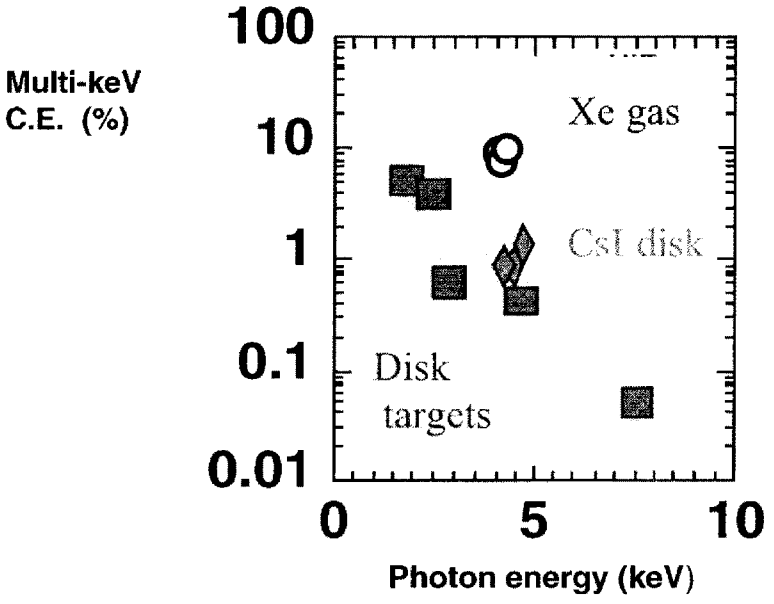

FIGURE 7. The conversion efficiency of disk targets and Xe targets.

Since L-shell conversion efficiencies have not been as extensively investigated as K-shell or M-shell conversion efficiencies, we undertook the comparison study of the slab conversion efficiency with beams spatially smoothed using KPP phase plates. These CsI experiments were performed with the same diagnostics as those used for the Xe-filled Be cans. They were performed by irradiating a slab target which had 6 μm of CsI coated on each side.

Past research has been difficult to reconcile with simulations because the experimental laser intensity was difficult to model. Due to limited energy available at laser facilities, the laser intensity was varied by changing the spot size. Also,

although beam image relaying techniques improve the spatial beam profile, the actual spatial intensity profile still contains hot spots unique to each beam.

In this study we improve both of these experimental limitations. KPP phase plates [19] were used to smooth the beams by eliminating > 10 μm-sized hot spots in the spatial profile and to define a 400 μm FWHM spot for each individual beam on target. The dependence of the conversion efficiency on laser intensity was investigated by varying the laser energy for a given spot size. The dependence of the conversion efficiency on source size was experimentally investigated by varying the overlap of the beams. The dependence of the conversion efficiency on laser intensity was investigated by varying the laser energy for a given spot size.

Since simulations typically employ a smooth envelope to model the spatial distribution of the laser beam intensity and not the far field intensity profile of the beam itself, these solid disk measurements discussed here provide a cleaner comparison to simulations than the typical reported data of this kind.

For the CsI solid target experiments, Fig 8 show a plot of conversion efficiency as a function of laser intensity. We also show predictions from calculations of these

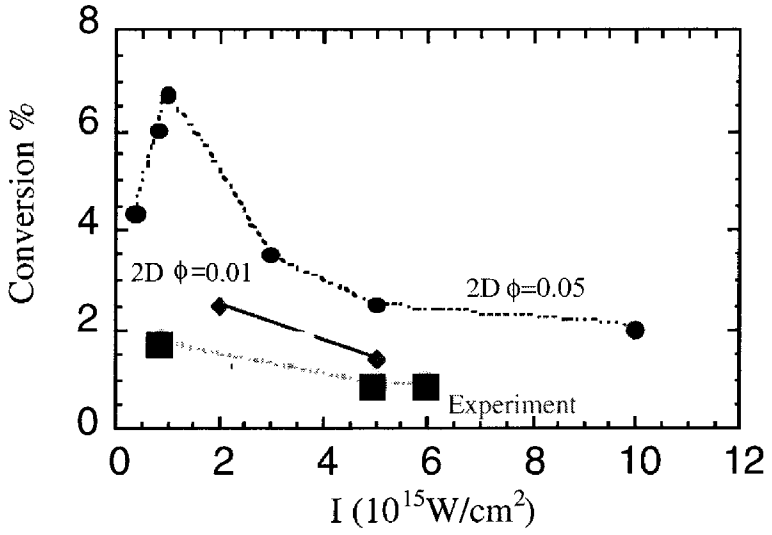

FIGURE 8. Conversion efficiency measured as a function of intensity for CsI disk targets as compared to 2-dimensional simulations.

experiments. Calculations using two different flux limiters,Φ, in two-dimensional simulations give significantly different results. These flux limiters span a reasonable range for modeling ICF targets [20]. Physically, a higher flux limiter

corresponds to a longer length of conduction region. These simulations are over a factor of two lower than the one-dimensional simulations. However, the experimental results are still below the predictions from two-dimensional simulations.

CONCLUSIONS

New multi-keV sources have been developed on the Nova laser. These sources are underdense radiators that take advantage of bound-bound radiation to maximize emission in the 4-7 keV photon range. The method of production is by supersonic heating of a confined gas. This technique allows efficient ionization of high-Z atoms, with less energy expended in kinetic energy and parasitic sub-keV emission losses.

The radiators have well-defined, uniform source size which is advantageous for radiograph, material testing, and next-generation fluorescence-type diagnostics. Furthermore, applications of these types of sources can be very diverse. For instance, the targets are modular and for future NIF applications, they can be multiplexed to provide extended sources for irradiating large areas. Or with standardized laser and target conditions, they may become instrument calibration sources.

ACKNOWLEDGEMENTS

The authors would like to thank R. Kauffman, B. Hammel, F. Ze for crystal calibrations, and the Nova laser and target fabrication crews. This work was performed under the auspices of the U.S. Department of Energy by University of California Lawrence Livermore National Laboratory under contract No. W-7405-Eng-48 and is supported in part by the U. S. DTRA contract number IACRO 98-3064, Work Units 57424 and 57425 and contract MIPR-00-2010/6171 to the Naval Research Laboratory.

REFERENCES

1. Glendinning, S. G., et al., Phys. Plasmas 7, 2033 (2000);); Ze, F., et al., *J. Appl. Phys.* 66, 1937 (1989).
2. Lindl, J. D., *Phys. of Plasmas* **2**, 3933-4024 (1995) and references therein.
3. Sigel, R., Eidmann, K. Lavarenne, F. and Schmalz, R. F. *Phys. Fluids B* 2, 199 (1989); Eidmann, K., Schmalz, R. F. and Sigel, R. *Phys. Fluids B* **2**, 208 (1989).
4. Mochizuki, T., Yabe, T. , Okada, K., Hamada, M., Ikeda, N., Ikyokama, S. and Yamanaka, C., *Phys. Rev. A* **33**, 525 (1986).
5. Kauffman, R. L., Suter, L. J., Darrow, C. B., Kilkenny, J. D., et al., *Phys. Rev. Lett.* **73**, 2320 (1994).
6. Matthews, D. L., Campbell, E. M., Ceglio, N. M., et al., *J. Appl. Phys.* **54**,. 4260 (1983).
7. Phillion, D. and Hailey, C. J., *Phys. Rev. A* **34**, 886 (1986).
8. Kodama, R., Okada, K., Ikeada, N., et al., *J. Appl. Phys.* **59**, 3050 (1986).
9. Yaakobi, B., Bourke, P., McCrory, R., et al, *Opt. Commun.* **38**, 196 (1981).
10. Kauffman, R. L., "X-ray Radiation from Laser Plasma" in *Handbook of Plasma Physics*, vol. 3, eds. Rubenchik and Witkowski, pp. 111-162 (Elsevier Science, North-Holland, 1991) and references therein.

11. Burkhalter, P. G., Nagel, D. J., and Whitlock, R. R., Phys. Rev. A **9**, 2331, (1974).
12. Zigler, A., Lee, R. W., Kilkenny, J. D., Kolbe, G., and Nathel, H. *J. Appl. Phys.* **62**, 1671 (1987).
13. Kauffman, R. L., et al. ICF Quarterly Report 6 (2), 96, Lawrence Livermore National Laboratory, CA UCRL-LR-50021-96-2 (1996).
14. Suter, L. J., Kauffman, R. L., Davis, J. F. and Maxon, M. S., ICF Quarterly Report 6 (3), 96, Lawrence Livermore National Laboratory, CA UCRL-LR-105821-96-3 (1996).
15. Dawson, J. , Kaw, P. , and Green, B. , *Phys. Fluids* **12**, 875 (1969); Lindl, J. *Inertial Confinement Fusion*, Springer-Verlag, New York, 1998, chapter 8 and 11.
16. C. Decker, private communication.
17. Henke, B. L., Fujiwara, F. G., Tester, M. A., Dittmore, C. H. and Palmer, M. A., *J. Opt. Soc. Am. B* **1**, 828 (1984).
18. Keane, C. J., Hammel, B. A., Osterheld, A. L. and Kania, D. R., *Phys. Rev. Lett.* **72**, 3029 (1994).
19. Dixit, S. N., Feit, M. D., Perry M. D. and Powell, H. T., *Opt. Lett.* **21** , 1715 (1996).
20. Fabbro, R. Max, C., and Fabre, E., *Phys. Fluids* **28**, 1463 (1985).